Proceedings Paper:
Lord, C., Rongong, J., Kiley, A. et al. (2023) Retro-fit particle dampers for panels in space structures. In: Proceedings of the European Conference on Spacecraft Structures Materials and Environmental Testing (ECSSMET). 17th European Conference on Spacecraft Structures Materials and Environmental Testing (ECSSMET), 28-30 Mar 2023, Toulouse, France. ECSSMET, p. 68.

RETRO-FIT PARTICLE DAMPERS FOR PANELS IN SPACE STRUCTURES

Lord, Charles E. (1), Rongong, Jem A. (2), Kiley, Andrew (3), Terzioglu Furkan (4)

(1)(2)(4) *University of Sheffield, Department of Mechanical Engineering, Sheffield, S1 3JD, United Kingdom, c.lord@sheffield.ac.uk, j.a.rongong@sheffield.ac.uk, fterzioglu1@sheffield.ac.uk*

(3) *Airbus Defence and Space, Gunnels Wood Rd, Stevenage, SG1 2AS, United Kingdom, andy.kiley@airbus.com*

KEYWORDS

vibration control, dampers, friction, panels

ABSTRACT

The presented paper explores the use of discrete particle dampers (PDs) as a retro-fit solution for vibration control of structural panels in space structures. The damper enables the user to change the structures overall dynamical characteristics thanks to their inherent many tuning parameters such as particle volume fraction, individual particle size, and overall mass. damper can provide broadband control and can operate at a range of amplitudes and within a range of severe environments. Random and sine vibrations of varying amplitudes, up to 1kHz, are applied to investigate the change in resonant and damping behaviour from the PDs for both bending and torsion modes. A finite element model (FEM) was then used to determine the estimated damping through a first order Modal Kinetic Energy method. The experimental and FEM results were found to satisfactorily agree with each other. It was found that optimised PDs can contribute high levels of energy dissipation with damping ratios up to 10%. At the same time, providing an acceptable mass contribution making them not only an acceptable candidate for space structures, but also a retro-fittable option with minimal re-qualification by test.

1. INTRODUCTION

Sensitive space-borne payloads demand high levels of robustness to endure the launcher flight loads. These loads are in the form of harmonic, acoustic and shock excitations which interact with the dynamic characteristics of the entire structure. When qualifying space structures and hardware, it is not uncommon to encounter localised exceedances or response levels projected to exceed local or global integrity constraints. The most common qualification or flight environment where exceedances are observed are associated with acoustic loads. Such exceedances are noted as Spacecraft acoustic test measured power spectral density (PSD) responses versus the sub-system (equipment) random qualification heritage. One method of reducing these vibration levels is to increase the damping of critical vibration modes by adding specially designed damping elements. The ability to retro-fit such devices is beneficial if potential vibration problems are detected late in the development programme ultimately reducing the need for re-qualification or alternatively the possibility of re-qualification by analyses. Viscoelastic polymers, which are used extensively in damping in a wide range of applications, are not easily integrated in space structures because of the need to minimise outgassing and to demonstrate survival when exposed to radiation and extreme temperatures. In addition, such materials are often associated with additional procurement cost resulting form process procurement management as well as environmental conditioning prior to delivery. In comparison to a compact PD system, certain visco-ealstic damping systems present potentially large footprints. PDs, comprising of small metal particles in a rigid container, offer a viable alternative that is more suitable for the space environment. Previously, dampers have been created by filling honeycomb sandwich panels with particles. However, this requires incorporating the particles early in the manufacturing stage of the panel rather than as a retro-fit solution for a ‘fix’. This research study looks at the use of discrete PDs that can be attached to structures that have already been built.

2. PARTICLE DAMPERS AND THEIR MANY REGIMES

Unlike with most types of dampers, where damping capacity is driven by the level of strain, PDs rely on the kinetic energy imparted onto them. PDs, in their simplest form, are elaborated multi-impact dampers containing several particles in an enclosure as shown in Fig. 1.

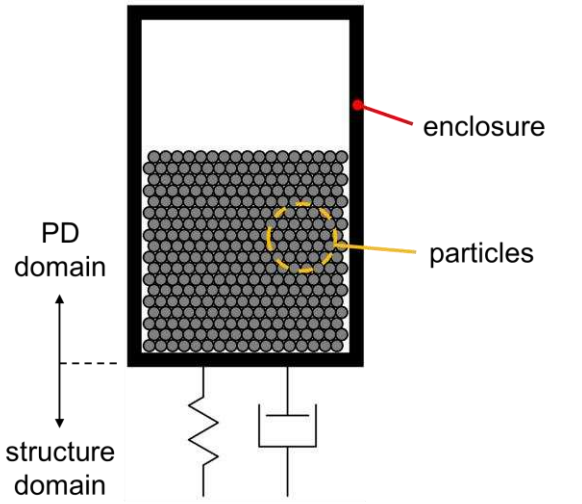

Figure 1: Typical particle damper arangement

Due to the fact that the energy dissipating mechanisms originate from inelastic impacts and friction, these types of dampers are highly nonlinear. As such, PDs, alongside most frictional type dampers, have an optimum operating amplitude, in the case of PDs also the frequency. This is illustrated in Fig. 2.

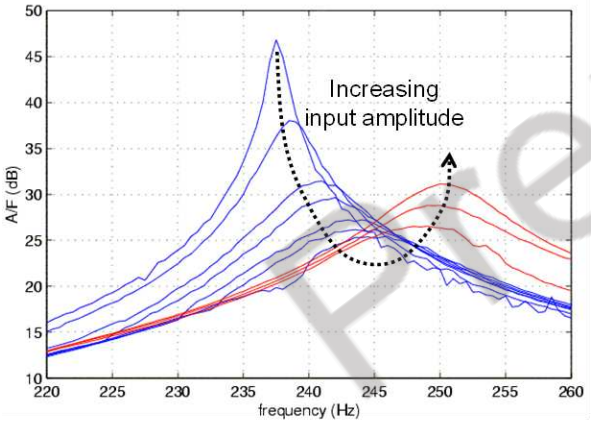

Figure 2: Inertance FRFs for an arbitrary PD demonstrating nonlinearity

When vibrationally excited at the right frequencies and amplitudes, the particles can move relative to one another and/or to the enclosure. This relative motion results in a complex combination of inelastic impacts and frictional sliding dissipating the excitation energy. As with most systems, the amount of dissipated energy is dependent on both the forcing frequency and amplitude. PDs however provide a unique case where many different physical motional phases can coexist for a specific frequency or amplitude. Of particular importance is the role that gravity plays as it is the parameter that controls the normal forces from particle-to-particle and particle-to-enclosure and is a major factor that controls the resistance forces against the particle decompaction. Fig. 2 demonstrates the various phases for PDs as a function of excitation frequency and the non-dimensional acceleration amplitude of harmonic excitation, Γ.

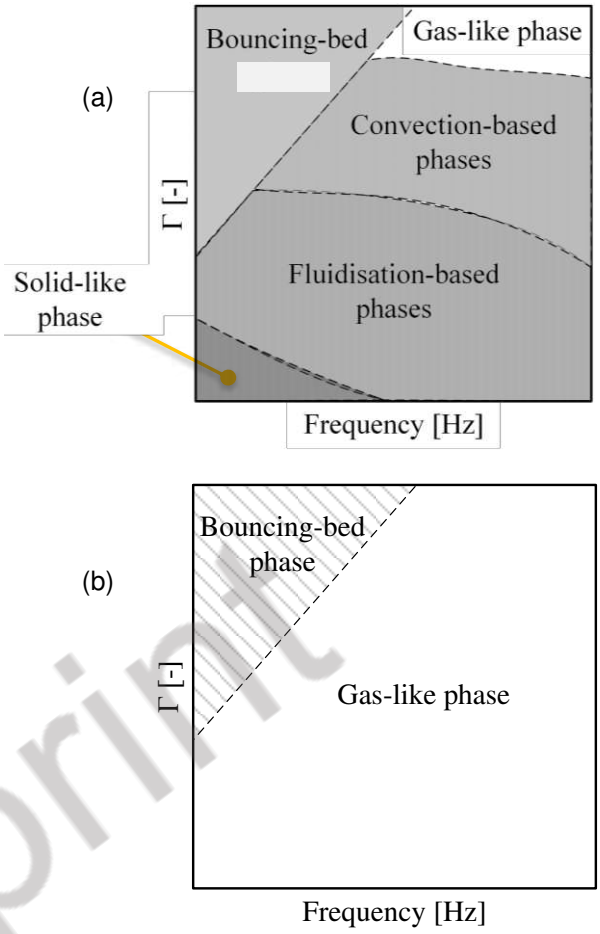

Figure 2: Motional phase maps for PDs under (a) gravitational loading and (b) absence of gravity

From the motional phase maps, five primary phases are identified. The 'Solid-like phase' is where the particle bed remains as a single mass that does not move relative to the enclosure and therefore dissipates a negligible amount of energy. In the 'Bouncing-bed' phase, the particles, while still fully assembled, move as a single mass relative to the enclosure and collide with the ends of the container. These collisions dissipate significant amounts of energy. As the frequency is increased, a 'Fluidisation-based phase' appears. This phase maintains the overall relative position for each of the particles with respect to one another but does contain relative motion. This type of motion can take place either locally within the particle bed or globally throughout. With either case, appreciable amounts of energy are dissipated over a wide range of frequencies. Additional energy provided to a PD will result in a 'Convection-based phase'. In this phase the particles change their contacts and move in varied patterns relocating their position relative to their original positions. Sub-categories within this phase, such as Leidenfrost effect and buoyancy convection depend on the type of particle flow motion that is observed. Generally, this motional

phase dissipates only small amounts of energy. At high levels of input energy, a 'Gas-like' phase is present. In this phase the particles are fully decoupled moving independently from neighbouring particles. In this phase the amount of energy dissipated relative to the input energy is relatively small. This is largely due to the fact that the input energy required to activate this phase is so large.

3. TEST VEHICLE

3.1. Panel

As a test vehicle, flight qualified surrogate honeycomb panels were supplied by Airbus Defence and Space (ADS) that would be used to carry out both the experimental and numerical investigations for purposes of this study. The panels are typical of those which would normally contain attachment instrumentation. The geometric size of the panel is provided in Fig. 3.

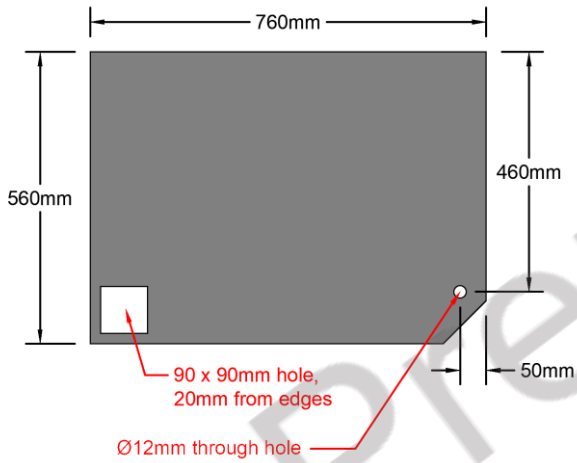

Figure 3: Honeycomb panel used as test vehicle for both experimental and numerical investigations

The honeycomb panel is composed of a Hexcel Corporation 5056 aluminium honeycomb core (T3.1-3/16-10P), nominally 20mm in thickness, sandwiched by a 2024-T81 aluminium face skin nominally 0.2mm on each of the footprint surfaces.

The constituent material properties for the material making up the face skins and honeycomb core are provided in Tab. 1. The total panel mass was 0.88 kg.

Table 1: Nominal properties for the material used in the honeycomb panel face skins and core (bulk properties are defined in Tab. 5)

Property	Units	Value
ρ	kg/m^3	2640
E	GPa	71
G	GPa	26.69
ν	-	0.33

3.2. Particle Damper

A cylindrical PD was chosen for this study. The details for the PD enclosure and particles are provided in Tab. 2.

Table 2: Particle damper dimensions and properties

	Parameter	Units	Value
Enclosure	Material	-	Perspex
	Height	mm	31.6
	OD	mm	50.6
	ID	mm	46.0
	Inner Depth	mm	22.1
	E	GPa	3.5
	ρ	kg/m^3	1180
	ν	-	0.35
Particles	Material	-	steel
	OD	mm	0.8
	ρ	kg/m^3	7870
	ν	-	0.30
	E	GPa	200
	Vol fraction	%	~93

The total mass of the PD used was 187g.

4. METHODOLOGY OF STUDY

4.1. Experimental Approach

The experiments for this study consisted of a combination of freely supported (hanging) impact hammer and shaker tests. The purpose for the hammer tests were to get an approximation for the first few natural frequencies. Impact hammer tests are good for initially identifying modal properties but are limited to generally linear structures. Shaker tests were performed with the honeycomb panel in both horizontal (parallel to the ground) and vertical (perpendicular to the ground) configurations. The typical setup is provided in Figs. 4-5.

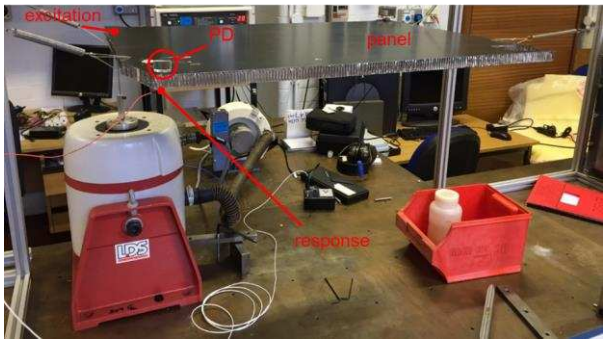

Figure 4: Shaker excited PD horizontally suspended configuration

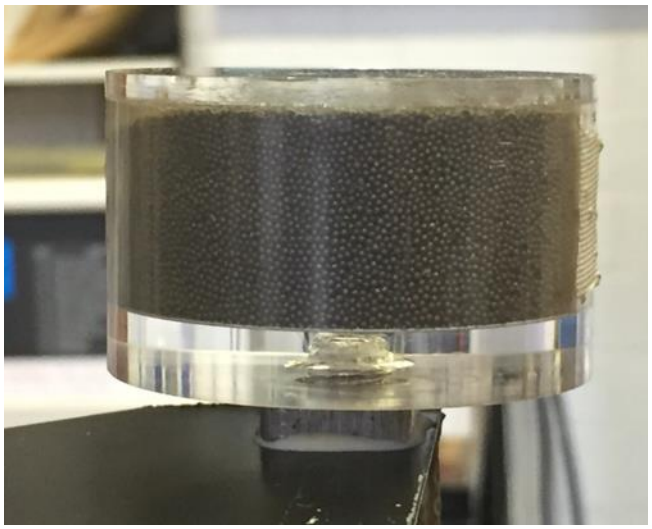

Figure 5: Closeup view of PD from Fig. 4

In these tests, the honeycomb panel was first excited with a random excitation to identify the natural frequencies and then stepped sine tests were performed to provide higher levels of energy into the structure. The random bandwidth was limited to 1kHz with a constant power spectral density for each of the random amplitudes considered. For the stepped sine tests, a tracking bandpass filter of 50Hz centred about the excitation frequency was used to minimise the noise from adjacent frequencies. The frequency resolution used was 0.32Hz with a dwell time for each frequency of 0.128s. The equipment used during the testing is outlined in Tab. 3.

Table 3: Constituent nominal material properties for honeycomb panel core and face sheets

Equipment	Model
Impact hammer	Dytran 5800B8
Electrodynamic shaker	LDS V455
Amplifier	LDS PA 1000L
Accelerometer	Dytran 3032A
Force sensor	Dytran 1053V3
Signal conditioner	Dytran 4102C/SigLab
Data acquisition	Picoscope 4224/SigLab

4.1.1. Panel Linearity Check

As part of the checkout process for the setup, the panel linearity was evaluated. Frequency response functions (FRFs) were measured prior to adding the PD. It was observed that the panel contained some nonlinearities which are estimated to be related to debonding artefacts between the honeycomb core and the face skins. This nonlinearity is shown in Fig. 6.

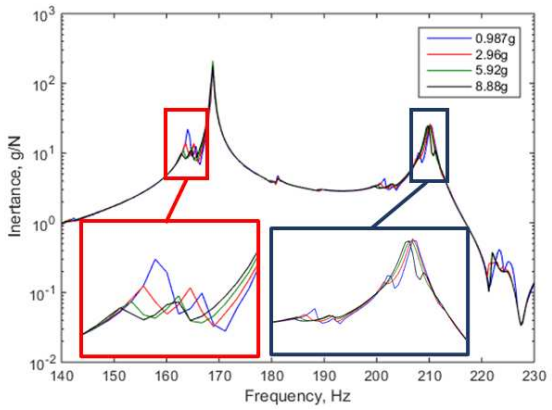

Figure 6: Neat honeycomb panel FRFs for first torsion mode (red) and first bending mode (blue)

Damping ratios were extracted from the FRFs (in Fig. 6) using the Kennedy–Pancu method. The results are provided in Tab. 4.

Table 4: Neat honeycomb panel first torsional and bending mode natural frequencies and damping ratios for various excitation amplitudes

	Amplitude (g)	f_n (Hz)	Damping Ratio (%)
Torsion	0.986	169	0.08
	2.96		0.08
	5.92		0.09
	8.88		0.09
Bend	0.986	210	0.23
	2.96		0.26
	5.92		0.29
	8.88		0.24

4.2. FEM Approach

4.2.1. Modelling and validation

A FEM of the honeycomb panel, according to Fig. 3, was produced using ANSYS commercial FE software. The FEM consists of three bodies: upper and lower face skins and the honeycomb core. The face skins were assumed to be made from a linear-elastic isotropic material having the properties defined in Tab. 1. Due to the complexity of the honeycomb structure, to reduce computational expense, a simplified model, where the honeycomb core is modelled as a solid orthotropic mass, was created using established analytical equations [1]. The density is therefore given by

$$\rho^* = \rho_S \frac{\frac{t}{l}\left(\frac{h}{l}+2\right)}{2\cos\theta\left(\frac{h}{l}+\sin\theta\right)}, \qquad (1)$$

where ρ_S is the constituent material density, t is the wall thickness of the honeycomb cells, h and l are the cell heights and θ is the interior orientation angle of the cell wall. For a regular hexagon, which is the case for the honeycomb panels used, $h = l$ and $\theta =$

30°. The modulus of elasticity for the in-plane (x and y axes) direction and out-of-plane (z-axis) direction are calculated using Eqs. 2-3, respectively.

$$E_x = E_y = E_S \left(\frac{t}{l}\right)^3 \frac{\cos\theta}{\left(\frac{h}{l} + \sin\theta\right)\sin^2\theta} \qquad (2)$$

$$E_z = E_S \left(\frac{t}{l}\right) \frac{\frac{h}{l} + 2}{2\left(\frac{h}{l} + \sin\theta\right)\cos\theta} \qquad (3)$$

E_S is the material modulus of elasticity for the constituent material. The shear moduli in the xy, xz and yz planes are respectively calculated using Eqs. 4-5.

$$G_{xy} = E_S \left(\frac{t}{l}\right)^3 \frac{\frac{h}{l} + \sin\theta}{\left(\frac{h}{l}\right)^2 \left(1 + 2\frac{h}{l}\right)\cos\theta} \qquad (4)$$

$$G_{xz} = G_{yz} = G_S \left(\frac{t}{l}\right) \frac{\frac{h}{l} + \sin\theta}{\left(1 + 2\frac{h}{l}\right)\cos\theta} \qquad (5)$$

G_S is the material shear modulus of the constituent material.

The constituent material properties used were taken from Tab. 1. Using Eqs. 1-5, equivalent linear-elastic material properties are derived for the honeycomb core and are identified in Tab. 5.

Table 5: Honeycomb core equivalent material properties

Property	Units	Value
ρ^*	kg/m^3	49.70
$E_x = E_y$	GPa	1.30E-4
E_z	GPa	0.75
G_{xy}	GPa	3E-5
$G_{xz} = G_{yz}$	GPa	0.137
$\nu_{xy} = \nu_{xz} = \nu_{yz}$	-	0

Poisson's ratios in the xy, xz and yz planes were set to 0. When calculated, these were a non-zero value but created a non-positive definite matrix. Adjusting the Poisson's ratios to non-zero values (where a positive definite matrix was valid) and comparing to Poisson's ratios of 0 had insignificant differences in the results.

Each of the bodies is modelled using 3-D SOLID186 higher-order hexahedral elements consisting of approximately 393,000 degrees of freedom. The maximum element aspect ratio was 50:1 for the face skins. A structured mesh was utilised for all the bodies to enforce contact between the core and face sheets. The Block Lanczos eigenvalue solver was applied as a resultant of the model nodal size and its robustness.

To validate the FEM, a set of modal hammer tests were carried out at 20 distinct locations. The honeycomb panel was suspended using nylon line and springs to represent free boundary conditions. From each test, the modal information was obtained. Fig. 7 shows the experimental FRFs obtained.

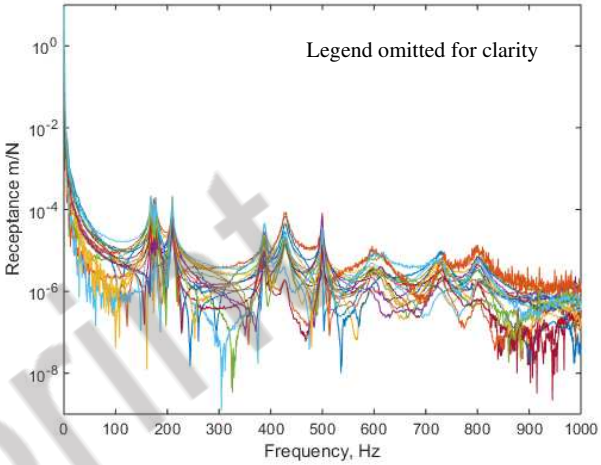

Figure 7: Experimental FRFs for free-free honeycomb panel

Tab. 6 shows the natural frequencies of the first 6 flexible modes, obtained experimentally and with the FEM. There is good agreement for the first two modes, but there is a divergence for the higher modes. Changing the material properties from those calculated in Eqs. 2-5 helped reduce the difference for the higher modes to within 5% but had a detrimental effect on the first torsional and bending modes. This study was not pursued further since the first two modes were thought to be the most important modes to damp.

Table 6: Experimental and FEM modal frequencies

Mode	Mode shape	Experiment (Hz)	FEM (Hz)	% diff
1	Torsion	168	163	3.0
2	Bending	210	205	2.4
3	Torsion	388	334	13.9
4	Bending	428	359	16.1
5	Torsion	500	402	19.6
6	Bending	600	462	23.0

Based on the close comparison between mode shapes and natural frequencies, for the experiments and the FEM, for modes 1 and 2, the FEM is considered to be validated.

4.2.2. FEM Implementation

Two configurations of PDs were studied. The first configuration was that of a single PD placed on one corner of the honeycomb panel. As the single PD introduces a bias on one corner of the honeycomb panel, the second configuration was that of four PDs distributed over four corners of the honeycomb panel to largely balance out the bias. The second configuration has the added advantage of the PDs spread in areas of high velocity (high kinetic energy). The location of the PDs for both configurations can be seen in Fig. 8; the PDs are highlighted in green.

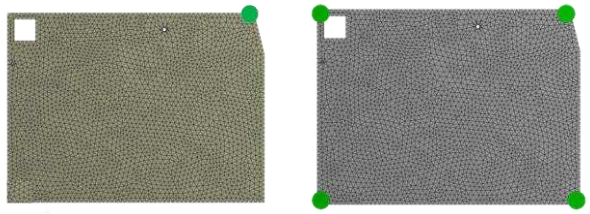

(a) (b)

Figure 8: FEM for (a) single PD and (b) four distributed PDs

Comparing the single PD to the four distributed PDs configuration, the total mass of the particles was maintained. However, as three additional containers were required to house the particles, the total mass of the latter configuration was slightly higher.

The honeycomb panel structures typically support equipment and other payload during launch and while in flight. Due to the high nonlinearity of PDs, the coupling effects from mass loading were also predicted. For each PD configuration, masses equivalent to 50kg/m^2 and 100kg/m^2 were applied to the entire structure by increasing the density of one of the face sheets.

4.2.3. Analysis Approach

The physics of PDs is typically modelled using the discrete element method (DEM), which captures the dynamics of the individual particles and its interaction with other neighbouring particles and the container. FEM can be used to provide a first approximate for the effects that PDs have on a structure by probing the kinetic energy distribution. The vibrational loss factor (2x critical viscous damping ratio) provided by PDs can be calculated using a modal strain energy approach as stated in Eq. 6.

$$\eta_s = \left(\frac{KE_{PD}}{KE_{total}} \right) \eta_{PD} \qquad (6)$$

where KE_{PD} and KE_{total} are the kinetic energies in the particle damper and the whole structure, respectively and η_{PD} is the loss factor of the PD. There is a range of values for η_{PD} used in previous research depending on the PD configuration (particle constitution, particle size, container size and particle pressure distribution). The absolute value is determined either through DEM analysis or by experimental characterization. The peak value for a particular damper generally ranges from 0.4 to 0.8. For the PDs used in this work, η_{PD} = 0.5.

5. RESULTS AND DISCUSSIONS

5.1. Experiments

5.1.1. Vertically suspended orientation

The honeycomb panel was excited with random vibrations at 2.14g$_{RMS}$ and 6.23g$_{RMS}$, up to 1kHz, to observe the change in resonant behaviour and gain an idea for the range of frequencies to be used in the stepped sine tests for the first torsion and first bending modes. Once the frequency ranges were determined, stepped sine tests were performed for a range of acceleration-controlled amplitudes (0.987g to 8.88g). The results from these experiments are provided in Figs. 9-10 and consolidated in Tab. 7. Like in Section 4.1.1, the damping ratios were extracted from the FRFs using the Kennedy–Pancu method. Each resonance is assumed to act as a single degree of freedom and a best fit circle is used for the experimental data to represent viscous damping.

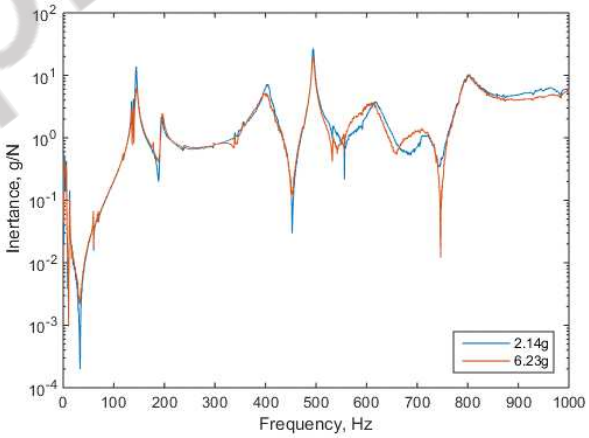

Figure 9: Random vibrations inertance FRFs for cylindrical PD, vertically suspended

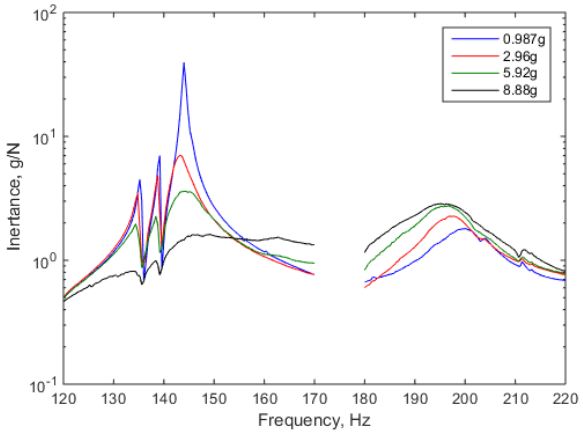

Figure 10: Stepped sine inertance FRFs for cylindrical PD, vertically suspended

Table 7: First torsional and bending mode natural frequencies and damping ratios for various excitation amplitudes, vertically suspended

Mode	Acceleration (g)	f_n (Hz)	Damping Ratio (%)
First Torsion	0.987	144	0.2
	2.96	143	1.1
	5.92	144	2.2
	8.88	143	5.3
First Bend	0.987	200	2.7
	2.96	197	2.5
	5.92	197	2.8
	8.88	197	3.6

In Tab. 8, from Fig. 10, the natural frequency and damping ratio values for the torsion mode are made in reference to the highest peak for each respective amplitude between the three torsion modes. The bending mode occurs between 197 and 200 Hz. It can be deduced that the cylindrical PD does have an effect on reducing the vibration levels in torsion at high levels of vibration amplitudes, as all three torsional mode peaks reduce, with a damping ratio of 5.3% achieved at 8.88g acceleration. The damping levels for the bending mode increase with acceleration levels also. However, the overall amplitude of the FRF tended to increase. The natural frequency for the first bending mode tends to decrease with increasing input amplitude. This is not a classical characteristic for PDs. It is believed that this originates from the panel nonlinearity as shown in Fig. 6. At low amplitudes, the core and the skins are sticking and hence, the honeycomb panel is stiffer. As the amplitude increases, the skins and core begin to slip, causing a reduction in stiffness. The reason that the PDs are more effective in torsion than in bending is attributed to the observed localised rocking motion where the PD is attached. PDs are most efficient when the motion is translational (i.e. in-plane and out-of-plane) and not rotational (i.e. rocking).

5.1.2. Horizontally suspended orientation

Using the same approach as in Section 5.1, the random and stepped sine vibration results can be seen in Figs. 11-12, respectively and the natural frequencies and damping ratios are provided in Tab. 8. The excitation levels for both the random and stepped sine tests were retained from the vertically suspended honeycomb panel tests in Section 5.1.

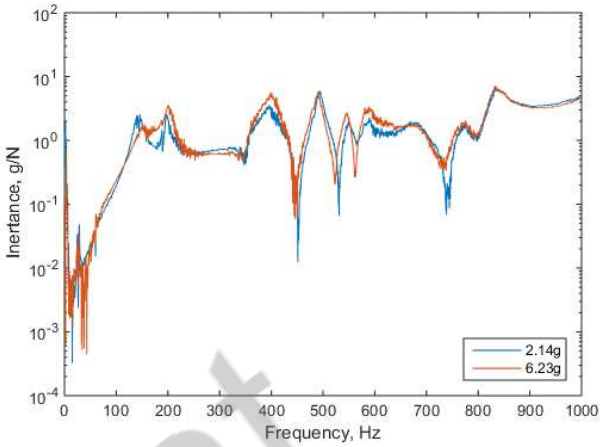

Figure 11: Random vibrations inertance FRFs for cylindrical PD, horizontally suspended

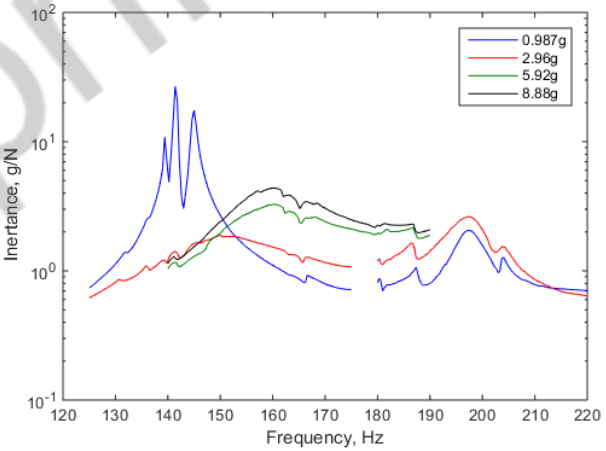

Figure 12: Stepped sine inertance FRFs for cylindrical PD, horizontally suspended

Table 8: First torsional and bending mode natural frequencies and damping ratios for various excitation amplitudes, horizontally suspended

Mode	Acceleration (g)	f_n (Hz)	Damping Ratio (%)
First Torsion	0.987	142	0.2
	2.96	148	6.3
	5.92	161	4.4
	8.88	160	3.9
First Bend	0.987	197	1.3
	2.96	198	1.8

In Tab. 8, from Fig. 12, the natural frequency and damping ratio values for the torsion mode are made in reference to the highest peak for each respective amplitude between the three torsion modes. The

bending mode occurs between 197 and 198 Hz.

The results of this set of tests indicate the classic trend of PD behaviour when operating in the Fluidisation phase, whereby damping increases with excitation, up to a peak value before reducing. At the same time, the natural frequencies increase with amplitude. At low amplitudes, the PD acts as a single solid ('solid'-like phase). Once excited to a high enough amplitude, some particles begin to overcome the gravitational force, whereas others are still in contact with the structure. There is a noticeable improvement in damping when moving from the vertical to horizontal orientation. For example, at 2.96g, the damping ratio increases from 1.1%, in the former, to 6.3%, in the latter. This is attributed to the improvement in pressure distribution in the horizontal orientation, with a reduction in local pressure concentration within the particles. Note that the 'Bouncing bed' is not experienced in this study because the frequencies of operation are high considering the fill ratio in the damper cavity.

5.2. FEM

Comparisons between a single PD and 4 distributed PDs having the same number of particles is provided in Tab. 9.

Table 9: Natural frequencies and damping ratios for various PD configurations and mass loadings

Mode	Config	Mass loading (kg/m^2)	f_n (Hz)	Damping Ratio (%)
Torsion	1 PD	0	135	5.3
		50	39	1.4
		100	29	0.7
	4 PD	0	101	9.8
		50	37	1.1
		100	27	0.6
Bend	1 PD	0	220	0.88
		50	48	0.3
		100	34	0.18
	4 PD	0	162	6.31
		50	45	0.45
		100	33	0.23

6. PD IMPLEMENTATION

It is often, from a sizing standpoint, that a specified reduction in vibration is sought. In this case, one would be interested in defining the desired equivalent damping coefficient, c_{eq} which can be compared to a characterized PD either via DEM analysis or experimentally. It is firstly important to study the mode shape(s) of the structure to be targeted and select initial placement of the damper unit(s). Particle dampers rely on *KE* to function, therefore optimal placement generally arises where the *KE* is greatest. One caveat to this however is that since PDs are nonlinear, it may appear sensible to move their location to positions where the vibration level is lower. PDs are capable of broad bandwidth damping, it might be of interest to damp several modes. It then becomes the task of considering the relevant mode shapes simultaneously. Placement can be achieved a number of ways including superimposing mode shapes to avoid modal nodes and to assess the highest summation of velocity.

The vibrational loss factor provided by PDs can be calculated using a Modal Kinetic Energy method. The modal mass is described by mass, M_n, and modal stiffness, K_n, are calculated for the modes to be damped, as these affect the mass of particles required. The modal properties should be normalised such that the associated mode shape vector has a maximum resultant magnitude of unity. The kinetic energy of a structure is extensive and can be described by the summation of both the translational and rotational components of kinetic energy according to,

$$KE = \frac{m}{2}\left(\sum \dot{x}^2\right) + \frac{I}{2}\left(\sum \omega^2\right) \qquad (7)$$

where m is the mass of the structure, $\dot{x}$ is the translational velocity, I is the moment of inertia of the structure, and ω is the angular frequency. For the particle damper, it is assumed that the motion occurs predominantly in a single axis (translationally) and that any 'rocking' or rotational motion is negligible meaning that the rotary term is ignored. This leads to the total kinetic energy for any mode being described by

$$KE_n = \sum_1^i \frac{m_{n,e}}{2}\left(\omega_n X_{n,e}\right)^2 \qquad (8)$$

where X is the modal displacement and subscript n is the mode number. From a finite element context, i is the largest element number in the finite element model and subscript e is the element number. The modal mass is described by

$$M_n = \frac{2KE_n}{{\omega_n}^2}\left(\frac{1}{\varphi_n}\right)^2 \qquad (9)$$

where φ_n is the greatest amplitude of mode shape deformation. The modal stiffness then is related to the natural frequency ω_n using,

$$K_n = {\omega_n}^2 M_n \qquad (10)$$

This damper is grounded at one end while the other is attached to the point where the particle damper is placed. The inherent modal damping of the neat structure, ζ_s,and the target damping ratio are required, ζ_n. As the damper may not be located at the point of maximum modal deflection, a scaling parameter, λ_n, is required. When it is reasonable to

assume that the mass of the particle damper does not change the mode shape significantly, this is obtained using,

$$\lambda_n = \left(\frac{\Phi_d}{\varphi_n}\right)^2 \quad (11)$$

where ϕ_d is the mode shape at the damper location.

If the damper is likely to alter the mode shape significantly, this scaling parameter can be estimated in a different way. The modal mass describes the portions of a structure that are in motion and contains kinetic energy. It is not uncommon for the kinetic energy of higher modes to be localised and decoupled from nearby mode shapes. The damping contribution from localised modal curvature can be estimated by

$$\lambda_n = \frac{\lambda_{n,\varphi}}{\max(\gamma_{n,\varphi})} \quad (12)$$

whereby taking the surface integral of the isolated mode shape as

$$\gamma_{n,\varphi} = \int_i^j \int_i^j KE_n(x,y)dxdy \quad (13)$$

where subscripts i and j denote the extreme boundaries along the in-plane 2-D surface. The required equivalent viscous damping coefficient required from the PD is described by,

$$c_{eq} = \frac{2\sqrt{K_n M_n}(\zeta_n - \zeta_s)}{\lambda_n \delta} \quad (14)$$

where ζ_s is the inherent damping ratio of the structure, ζ_n is the target damping ratio, and δ is used to adjust for the effects of the excitation normal direction of the PD with respect to standard earth gravity. The estimated magnitude of δ is ascertained from experimental data. While δ is independent of the particle material, it is dependent on the shape and configuration of enclosure.

The mass of particles required to achieve the required damping coefficient can be constructed through an acceleration dependent performance curve by taking averages between the different damping curves and dividing by the mass of the particles. This is shown in Fig. 13.

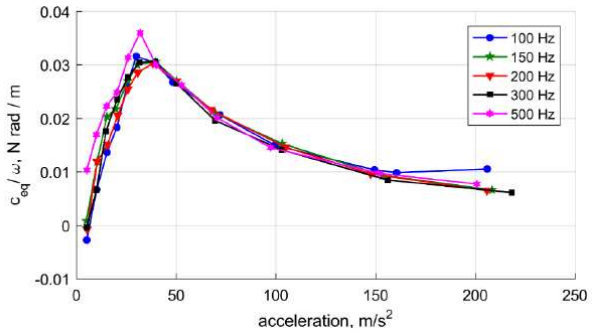

Figure 13: Typical acceleration dependent performance master curve

For each mode in question, the frequency of interest is the natural frequency ω_n, and the required damper coefficient c_{eq} is output from the performance curve as exampled in Fig. 13. The required mass of particles can be obtained if the acceleration level at the damper location is known as shown in Fig. 14.

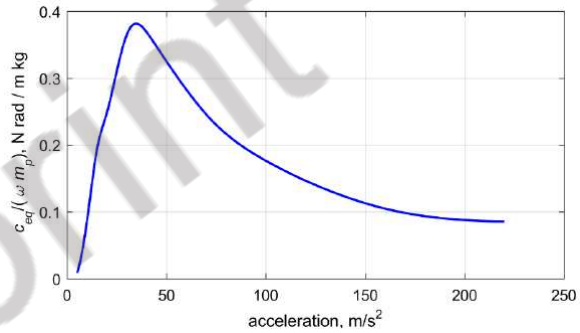

Figure 14: Damping performance $c_{eq}/(\omega_n m_p)$ as a function of acceleration

Dependent of the structure, it is likely that the addition of the particle damper will change the mode shape, resonant frequencies, modal mass, modal stiffness and therefore the required damping coefficient. It is therefore pertinent that eqs. 7-14 are reiterated until a converged performance master curve is achieved.

6.1. PD Implementation Validation

To validate the particle damper implementation process in Section 6, a FEM for a simple plate that is fixed-fixed is considered. The plate is steel (E=200GPa, ρ=7850kg/m^3 and ν=0.3) with dimensions of 425mm x 75mm x 4mm. A spherical particle damper centrally located with a fill ratio of 90.6%, with tungsten carbide particles having a total mass of 81g was considered. Two modes were considered: flexural mode 1 and flexural mode 3. Flexural mode 2 was not accounted for since the particle damper resides on a flexural mode 2 vibrational node and results in a 'rocking' motion only.

From the FEM, the results for the natural frequencies and absolute modal mass and absolute

modal stiffness are provided in Tab. 10.

Table 10: FEM results for plate characteristics

Mode	f_n (Hz)	Modal Mass (kg), M_n	Modal Stiffness (kN/m), K_n
1F	117	0.388	208
3F	630	0.396	6209

The validation followed the implementation process outlined in Section 6 while extracting the c_{eq} values from the damper characterisation tests in Fig. 15 (mode 1) and Fig. 16 (mode 3).

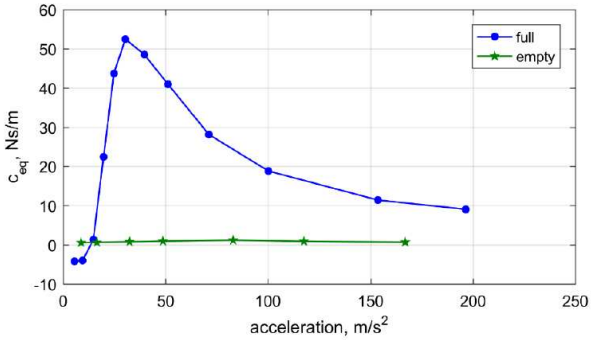

Figure 15: 200Hz excitation PD master curve

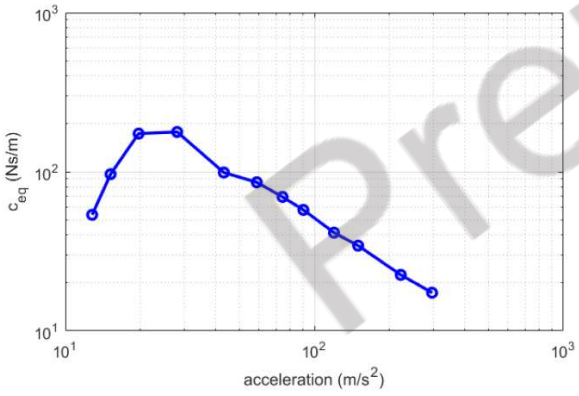

Figure 16: 645Hz excitation PD master curve

The comparison of damping ratio results is made in Tab. 11. For mode 1, the calculated damping ratio was directly compared to the test data. For mode 3, the calculated damping ratio was compared to a FEM using an appropriately located point mass and zero stiffness dashpot elements to represent the particle damper.

Table 11: Flexural mode 1 and 3 comparison of damping ratios between the suggested implementation process, test data and FEM

Mode	Implementation Process (Eqs. 7-14)	Test Data	FEM	Error
1F	4.84%	4.75%	3.73%	1.89%
3F	1.95%	-	3.06%	12.3%

It is shown that at for mode 1 the percent error is low but for mode 3 this increases. One possible reason would be the non-exact characterisation of the particle damper at these modal frequencies. For mode 1 there is a 0.1% difference between the characterisation frequency and the modal frequency whereas for mode 3 there is approximately a 9% difference.

7. CONCLUSIONS

A flight qualified surrogate honeycomb panel was used as a test vehicle to explore the use of the PDs as a vibration control approach. Tests with the PDs involved two orientations (the honeycomb panel suspended vertically and horizontally) and two different configurations for the horizontally suspended orientation. It was noted that the particles activated at lower input amplitudes for the horizontally suspended cases. This was because of gravity improving the pressure distribution.
PDs are highly nonlinear and highly optimisable due to their many parameters and broad bandwidth capability. Optimisation is required for different operating conditions such as excitation level, number of targeted vibrations modes to control, and location of modal kinetic energy.

A FEM of the panel was created using ANSYS commercial software. The modal characteristics of the model were validated by comparing the predicted results with a set of impact hammer tests carried out on various locations of the honeycomb panel. Good agreement was achieved, particularly for the first bending and torsion modes. The FEM explored the concept of lumped versus distributed PDs while maintaining the same particle mass. It was clear that the distributed PDs provided an advantage when mass loading was not accounted for. When uniform mass loading was added, the results were inconclusive. It is likely that the positioning of the PDs was not ideal for either scenario and the data should evaluated further before having a definitive conclusion.

The main findings from the PDs FEM study shows that:

- as mass loading increases, the mass for PDs also needs to be increased to achieve the same level of damping
- as the mass of the PDs increases, the level of damping also increases to a certain point, where it approaches an asymptote
- distributing a single PD into several PDs, having the same mass, increases the level of damping in most cases, when positioned correctly

As a point of interest, Fig. 15 shows an experimental comparison between FRFs for honeycomb panel alone (as received) and with independent scenarios

of equal mass PDs and CLDs subjected to random vibrations.

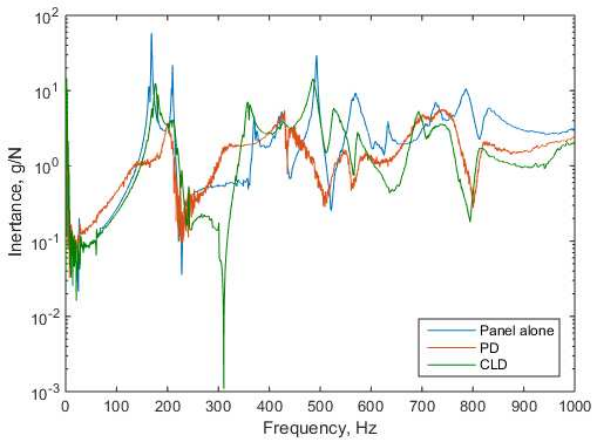

Figure 15: Random vibrations inertance FRF comparison between panel alone, PD and CLD

When comparing the three FRFs in Fig. 15, it is clear that the PD significantly reduces the vibration response of the first (torsion) mode by almost two orders of magnitude, whereas the damping increase caused by the CLD is just under one order of magnitude. The second (bending) mode is also suppressed by both damping approaches, almost equally. At higher modes, the CLD generally performs better to reduce the vibration magnitude. This supports the findings that PDs, although useful for broadband suppression, are excellent for narrow band suppression (optimised for particular amplitudes and frequencies), whereas CLDs provide consistent levels of damping over a wider bandwidth. It has been observed that PDs offer the same, or higher levels of damping when compared to CLDs of the same mass. In terms of damping/added mass ratios, PDs, if optimised correctly, would be the most suitable candidate.

An FEM implementation approach has been established where sizing a particle damper in terms of the equivalent damping coefficient is very possible. This offers a quick solution as a design tool to use and optimise the use of PDs despite their complex characteristics.

Note that the studies here were carried out on freely suspended panels for a combination of bending and torsion modes. However, the findings are generic for panel modes with significant out-of-plane deflection. Hence, it is reasonable to assume that the conclusions from this work are equally valid for example, for panels with clamped boundaries undergoing mainly bending type vibrations. In such a case, the damper locations would be moved to areas of highest modal deflection.

8. ACKNOWLEDGEMENTS

Thanks are expressed to Airbus Defence & Space UK for funding this research. The principal output of this research being to produce a design manual, with sizing parameters, centred on standard particle containers for retro-fit application.

9. REFERENCES

[1] Gibson, L.J. and Ashby, M.F., “Cellular Solids: Structure and properties”, 1999